Functional photoacoustic micro-imaging of rat cerebral hemodynamic response function in single vessels during forepaw electrical stimulation

Lun-De Liao[a,b,1], You-Yin Chen[c,1], Chin-Teng Lin[a,b], Jyh-Yeong Chang[a], Meng-Lin Li[c*]

[a]Department of Electrical Engineering, National Chiao Tung University, Hsinchu, 300, Taiwan

[b]Brain Research Center, National Chiao Tung University, Hsinchu, 300, Taiwan

[c]Department of Biomedical Engineering, National Yang Ming University, Taipei, 112, Taiwan

[d]Department of Electrical Engineering, National Tsing Hua University, Hsinchu, 300, Taiwan

[1] Equal contribution.
[*]Email: mlli@ee.nthu.edu.tw

ABSTRACT

The specificity of the hemodynamic response function (HRF) is determined spatially by the vascular architecture and temporally by the evolution of hemodynamic changes. Here, we used functional photoacoustic microscopy (fPAM) to investigate the spatiotemporal evolution of the HRFs of hemoglobin concentration (HbT), cerebral blood volume (CBV) and hemoglobin oxygen saturation (SO_2) in single cerebral vessels to rat left-forepaw stimulation. The HRF changes in specific cerebral vessels responding to different stimulation intensities and durations were bilaterally imaged with 36 × 65-μm spatial resolution. Various electrical stimulations were applied with stimulation intensities at 1, 2, 6 and 10-mA combined with 5-s and 15-s stimulation durations, respectively. Our main findings were as follows: 1) the functional HbT and SO_2 increased sub-linearly with increasing stimulus intensities and 2) the results suggested that the CBV changes are more linearly correlated with arterioles than HbT and SO_2 within a limited dynamic range of stimulation intensities and duration. The findings in this study indicate that the regulation of hemodynamic changes in single cerebral vessels can be reliable studied by the fPAM technique without the use of contrast agents.

Keywords: hemodynamic response function, functional imaging, photoacoustic microscopy, electrical stimulation, hemoglobin oxygenation.

1. INTRODUCTION

For understanding the hemodynamic response function (HRF) in single cerebral blood vessels, it is crucial to image changes in total hemoglobin concentration (HbT), cerebral blood volume (CBV) and hemoglobin oxygen saturation (SO_2). Recently, optical brain imaging has been increasingly used to study brain functions *in vivo* because it can measure oxy- (HbO_2) and deoxy-hemoglobin (Hb) through the distinctive optical absorption characteristics. Diffusion optical imaging (DOI) and laser speckle imaging (LSI) are the two most widely used optical imaging techniques for the *in vivo* imaging of cerebral hemodynamic changes. The DOI technique can directly acquire CBV, HbO_2 and Hb signals through the intact skull and track their changes noninvasively in response to an electrical stimulation of the rat forepaw. However, for DOI, SO_2 quantification is problematic due to tissue scattering and the nonlinear relationship between signal intensity and absorption coefficients[1-3]. This problem also impairs the visualization of HRF changes in single blood vessels. In contrast, LSI can probe the hemodynamic changes in single blood vessels with high spatial resolution after the skull has been removed[4]. However, due to the limited penetration depth and poor depth resolution of LSI, it can only access information from single blood vessels that reflect from the cortical surface[5-7].

Photons Plus Ultrasound: Imaging and Sensing 2012, edited by Alexander A. Oraevsky, Lihong V. Wang,
Proc. of SPIE Vol. 8223, 822334 · © 2012 SPIE · CCC code: 1605-7422/12/$18 · doi: 10.1117/12.908131

Functional photoacoustic microscopy (fPAM), which can measure functional hemoglobin changes in single blood vessels without a labeling agent, is ideal for the *in vivo* imaging of changes in HbT, CBV and SO_2. Recently, photoacoustic (PA) imaging has been applied to subcutaneous vasculature imaging[8], breast tumor detection[9] and oxygenation monitoring in blood vessels[10, 11]. Our recent study utilized the fPAM capability of acquiring relative functional hemodynamic responses to forepaw electrical stimulation in exposed rodent brains[12]. Our findings indicate that hemodynamic changes in specific cortical regions of the brain can be reliably imaged using fPAM.

In this study, we used fPAM to investigate the spatiotemporal evolution of the functional changes in hemoglobin concentration, cerebral blood volume and hemoglobin oxygen saturation in single cerebral vessels to rat left-forepaw stimulation. Those changes in specific cerebral vessels responding to different stimulation intensities and durations were bilaterally imaged with 36 × 65-μm spatial resolution. Various electrical stimulations were applied with stimulation intensities at 1, 2, 6 and 10-mA combined with 5-s and 15-s stimulation durations. Our findings indicate that the regulation of hemodynamic changes in single vessels can be reliable studied by the fPAM technique.

2. MATERIALS AND METHODS

2.1 Dark-Field Confocal Photoacoustic Microscopy System

A 50-MHz dark-field confocal fPAM system was used to image the functional changes in specific cortical vessels in this study. Laser pulses were generated by an optical parametric oscillator (Surlite OPO Plus, Continuum, USA) pumped by a frequency-tripled Nd:YAG Q-switched laser (Surlite II-10, Continuum, USA), which provides ~4-ns laser pulses at a pulse repetition rate of 10 Hz. Laser pulses at two visible wavelengths, 560 (λ_{560}) and 570 nm (λ_{570}), were used for PA wave excitation. To probe the relative changes in HbT, CBV and SO_2 in specific blood vessels, these two wavelengths have been optimized to provide high signal-to-noise ratios (SNRs) and sensitivity[12]. The 50-MHz ultrasonic transducer used in the current fPAM system was custom-made by the Resource Center for Medical Ultrasonic Transducer Technology at the University of Southern California (http://bme.usc.edu/UTRC/), offering an axial resolution of 36 μm and a lateral resolution of 65 μm.

Laser energy was delivered by a 1-mm multimode fiber. The fiber tip was coaxially aligned with a convex lens, an axicon, a plexiglass mirror, and an ultrasonic transducer on an optical bench, forming dark-field illumination that is confocal with the focal point of the ultrasonic transducer. The incident energy density on the sample surface was well within the safety limit of the American National Standards Institute (ANSI). During the imaging process, the transducer was immersed in an acrylic water tank with a hole in the bottom that was sealed with a piece of 15-μm-thick polyethylene film. A thin layer of ultrasonic gel was applied onto the rat's head and then attached to the thin film, in order to ensure good coupling of PA waves to the tank. The PA signals received by the ultrasonic transducer were pre-amplified by a low-noise amplifier (noise figure 1.2 dB, gain 55 dB, AU-3A-0110, Miteq, USA) and cascaded to an ultrasonic receiver (5073 PR, Olympus, USA). Then, the signals were digitized and sampled by a computer-based, 14-bit analog to digital (A/D) card (CompuScope 14200, GaGe, USA) at a 200-MHz sampling rate for data storage. The fluctuations in the laser energy were monitored by a photodiode (DET36A/M, Thorlabs, USA). Finally, the recorded photodiode signals were applied to compensate for PA signal variations caused by laser energy instability before any further signal processing.

2.2 Experimental animals

Six male Wistar rats (National Laboratory Animal Center, Taiwan) weighing 250–300 grams each were used. The animals were housed at a constant temperature and humidity with free access to food and water. Before the imaging experiments, the rats fasted for 24 hours but were given water *ad libitum*. All animal experiments were conducted in accordance with the guidelines of the Animal Research Committee of National Chiao Tung University and National Tsing Hua University. The animals were initially anesthetized with 3% isoflurane. Supplemental α-chloralose anesthesia (70 mg/kg) was injected intraperitoneally as needed. The anesthetized rats were mounted on a custom-made acrylic stereotaxic head holder, and the skin and muscle were cut away from the skull to expose the bregma landmark. The anteroposterior (AP) distance between the bregma and the interaural line[13] was directly surveyed. The bregma was 9.3 ± 0.12 mm (mean ± standard deviation [SD]) anterior to the interaural line[14]. Next, a craniotomy was performed on each animal, and a bilateral cranial window of approximately 8 (horizontal) × 6 (vertical) mm was made with a high-speed drill. After the rat was secured to the stereotaxic frame and placed on the bed pallet, the pallet was moved into position at

the bregma, which was 9 mm anterior to an imaginary line drawn between the center of each ear bar (the interaural line)[12]. In the subsequent experiments, the interaural and bregma references were then used to position the head in the fPAM system without additional surgery.

After bregma positioning, a PA C-scan was performed to acquire reference images of the cortical vasculature. The cortical blood vessels were imaged *in vivo* by fPAM at λ_{570}, as shown in Figure 1. In addition, arteriolar branches from the anterior cerebral artery (ACA) vessel system can be seen in the projected C-scan image[15, 16]. These were bilaterally identified as MI and MII and are labeled in Figures 1 along with the superior sagittal sinus (SSS). The SSS is the largest vein in the rodent brain cortex[16]. The MI and MII arterioles are two different-sized arterioles that branch from the ACA blood vessel system and extend from the bottom center of the brain to the cortical surface. The bilateral MI arterioles cross through the anatomical borders of the primary motor cortex and secondary motor cortex[16]. However, the bilateral MII arterioles are located in the anatomical borders of the primary somatosensory cortex that innervates the forepaw (S1FL) [16, 17]. Functional changes in HbT, CBV and SO_2 in the SSS and the bilateral MI and MII arterioles were imaged by fPAM scanning during stimulation. These images were acquired along the black solid and dashed lines in the bilateral regions shown in Figure 1. Moreover, some branches of these vessels were also visualized in the projected C-scan image.

2.3 Forepaw electrical stimulation

Forepaw stimulation was applied to evoke functional hemodynamic changes in the cerebral vessels, and it was achieved by insertion of thin-needle stainless electrodes under the skin of the rat's left forepaw. Electrical stimulation was then applied using a stimulator (Model 2100, A-M Systems, USA). A monophasic constant current of four pulses of different intensities (1, 2, 6, and 10 mA) with a 0.2-ms pulse width at a frequency of 3 Hz was used. Various stimulation intensities were employed to evoke hemodynamic changes of different strengths during the stimulation onset. In addition, two stimulation durations of 5 and 15 s were employed. A block-design paradigm was employed in this study for functional signal acquisition. The short stimulation duration (5 s) was originally selected to provide enough time for the hemodynamic response to reach a maximum value in order to enable the large amount of averaging necessary[18]. The longer stimulation duration (15 s) was selected to enable the cerebral volume response to reach a nearly maximal response while avoiding the progressive attenuation that is seen for stimuli of longer durations[19]. Each trial consisted of three blocks, and each block began with a 20-s baseline that was followed by a 5-s Stimulation-ON and a 75-s Stimulation-OFF period for the shorter stimulation or a 15-s Stimulation-ON and a 65-s Stimulation-OFF period for the longer stimulations. There was a 5-s lapse between each block, and the PA signals at λ_{560} or λ_{570} were acquired in each block to assess stimulation-induced hemodynamic changes in specific single cortical vessels (the SSS and bilateral MI and MII arterioles).

2.4 Data analysis of the functional changes in CBV, HbT and SO_2

Two optimized wavelengths (i.e., λ_{560} and λ_{570}) were employed to monitor functional HbT, CBV, and SO_2 changes. Functional CBV changes (R_{CBV}) in a single vessel can be monitored by assessing the changes in the cross-section of the vessel during each block against a cross-section baseline acquired immediately before the electrical stimulation onset (i.e., ~20 s in each block). PA cross-sectional B-scan images of each specific single vessel at λ_{570} (i.e., $I_{R(570)}$) were used. $R_{CBV}(t)$ was constructed according to the following equation:

$$R_{CBV}(t) = \frac{A(I_{R(570)}(t))}{A(I_{R(570),baseline})}, \tag{1}$$

where t is the time in each block, $A(I_{R(570)}(t))$ represents the cross-sectional area of a single vessel at a given time in each block, and $A(I_{R(570),baseline})$ is the cross-section baseline estimated from the baseline image acquired immediately before electrical stimulation onset in each block. $A(I_{R(570)})$ was calculated from the total vessel pixel count of a single vessel image (i.e., $I_{R(570)}$).

PA B-scan images at λ_{570} ($I_{R(570)}$) were used to probe the changes in HbT. Because the PA signal at a given pixel in $I_{R(570)}$ is proportional to the HbT within the PA resolution cell centered at that pixel, the mean functional HbT changes ($R_{\mathrm{HbT}}(t)$) in a single vessel during the stimulation period could be assessed as follows:

$$\begin{aligned} R_{\mathrm{HbT}}(t) = & \sum_{(x,z)\in \text{vessel pixel}} (I_{R(570)}(x,z,t)) / A(I_{R(570)}(t)) \\ & - \sum_{(x,z)\in \text{vessel pixel}} (I_{R(570),baseline}(x,z,t)) / A(I_{R(570),baseline}(t)) \end{aligned} \tag{2}$$

where (x, z) is the pixel position and $I_{R(570),baseline}$ is the baseline image at λ_{570} acquired immediately before electrical stimulation onset in each block.

Functional images of SO_2 changes ($\Delta I_{F(560)}(t)$) at the given time point t in each block were then assessed according to the following equation:

$$\Delta I_{F(560)}(t) = \frac{I_{(560)}(t)}{I_{R(570)}(t)} - \frac{I_{(560),baseline}}{I_{R(570),baseline}} = I_{F(560)}(t) - I_{F(560),baseline} \quad (3)$$

where $I_{(560)}$ (i.e., the PA image acquired at λ_{560}) was normalized to $I_{R(570)}$ on a pixel-by-pixel basis, and $I_{(560),baseline}$ was the baseline image at λ_{560} acquired immediately before electrical stimulation onset in each block. In this equation, negative values in $\Delta I_{F(560)}$ (i.e., a positive $-\Delta I_{F(560)}$) indicate increases in the SO_2 level and vice versa. The mean functional SO_2 changes ($R_{SO_2}(t)$) in a single vessel during the stimulation period were probed as follows:

$$R_{SO_2}(t) = \sum_{(x,z)\in \text{vessel pixel}} (I_{F(560)}(x,z,t)) / A(I_{R(570)}(t)) - \sum_{(x,z)\in \text{vessel pixel}} (I_{F(560),baseline}(x,z,t)) / A(I_{R(570),baseline}(t)) \quad (4)$$

When $I_{R(570)}$ is used as a marker for HbT and $I_{F(560)}$ is used as a marker for SO_2, the fPAM system can be used to probe the changes in HbT and SO_2 independently, as shown in Equations (2) and (4).

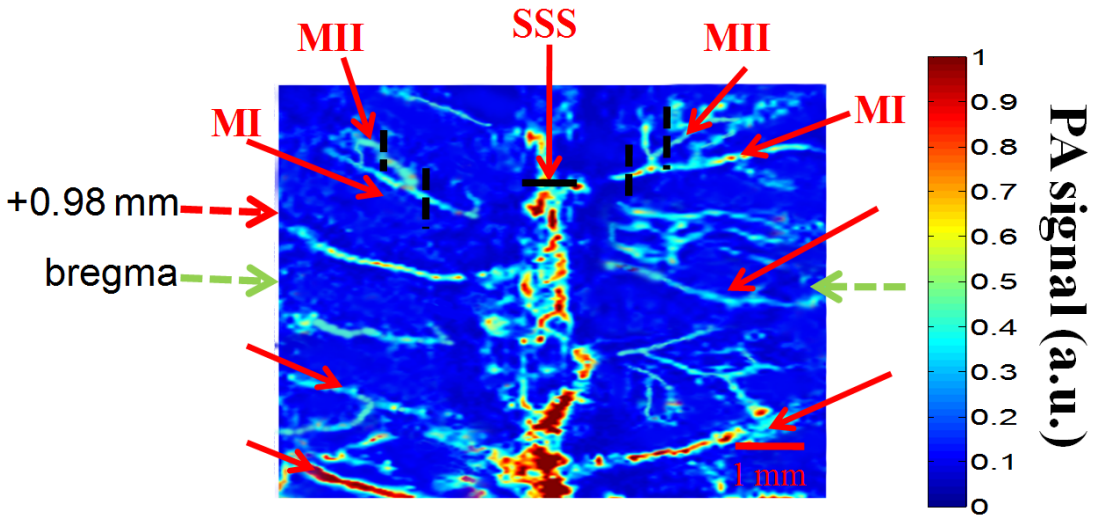

Fig. 1 *In vivo* PA-projected C-scan image of the blood vessels in the superficial layer of the cortex, acquired at λ_{570}. Some branches of the blood vessels, which are indicated by the red solid arrows, are imaged clearly. The green dashed line indicates the position of the bregma. The red dashed arrow indicates the section of the bregma + 0.98 mm activated during left forelimb stimulation. The superior sagittal sinus (SSS) and some cortical vessels on the cortical surface can be identified. Functional B-scan images of the SSS and bilateral MI and MII arterioles were acquired by scanning along the black solid and dashed lines in the bilateral region.

3. EXPERIMENTAL RESULTS

3.1 Functional hemodynamic changes in the bilateral cerebral vessels in response to various stimulation intensities

The first rows of Figures 2 and 3 show $R_{HbT}(t)$ in the SSS and bilateral MI and MII arterioles in one stimulation block and using the stimulation intensities of 1, 2, 6 and 10 mA, with a duration of 5 s. Significant HbT changes were observed in the SSS and MI and MII arterioles contralateral to the electrically stimulated left forepaw. In contrast, no significant HbT changes were found in the ipsilateral MI or MII arteriole. The time to peak R_{HbT} in the SSS and the contralateral MI and MII arterioles after stimulation onset using a stimulation intensity of 2 mA was 16.24, 9.68 and

19.75 s, respectively. There was no significant difference among the times to peak R_{HbT} in the SSS or contralateral MI and MII arterioles using any of these stimulation intensities.

The second rows of Figures 2 and 3 show $R_{CBV}(t)$ in the SSS and bilateral MI and MII arterioles in one stimulation block under stimulation intensities of 1, 2, 6 and 10 mA and a stimulation duration of 5 s. Using a stimulation intensity of 2 mA, the time to peak R_{CBV} was 8.34 s in the contralateral MI arteriole and 16.13 s in the contralateral MII arteriole after stimulation onset. There was no significant difference in the time to peak R_{CBV} between the contralateral MI and MII arterioles using any of the four stimulation intensities; however, the peak R_{CBV} values were significantly different between the MI and MII arterioles.

The third rows of Figures 2 and 3 illustrate time course measurements of $-R_{\mathrm{SO}_2}$ in the SSS and bilateral MI and MII arterioles in one stimulation block using stimulation intensities of 1, 2, 6 and 10 mA and a duration of 5 s. After stimulation onset at 2 mA, the time to peak $-R_{\mathrm{SO}_2}$ was 12.14, 9.87 and 17.82 s in the SSS and contralateral MI and MII arterioles, respectively. There was no significant difference among the times to peak $-R_{\mathrm{SO}_2}$ in the SSS and the contralateral MI and MII arterioles when any of the four stimulation intensities were being used. However, the peak $-R_{\mathrm{SO}_2}$ values were significantly higher than baseline under these stimulation intensities. The peak $-R_{\mathrm{SO}_2}$ values changed in proportion to the stimulation intensity.

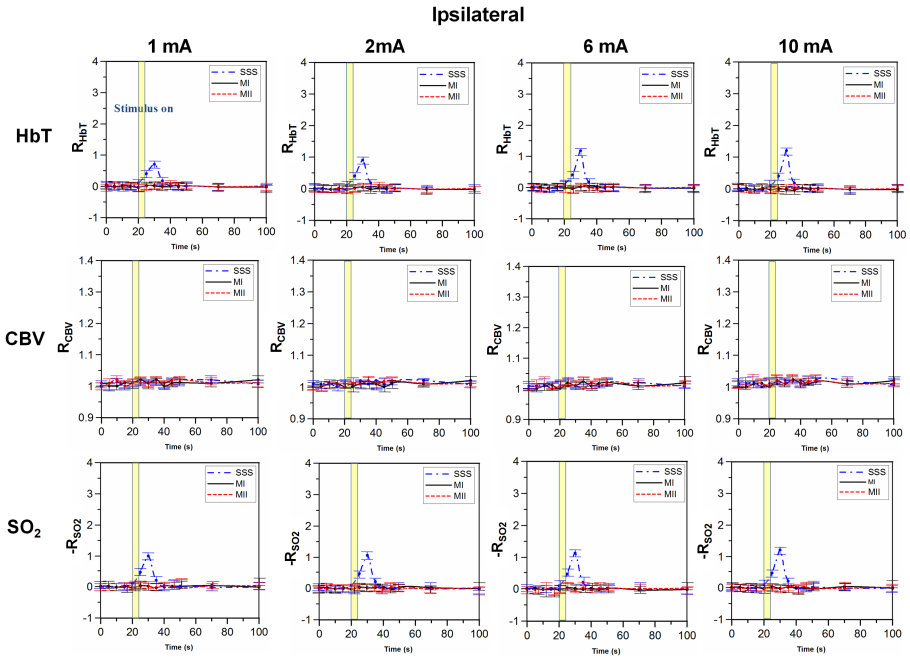

Fig. 2 Ipsilateral functional changes in the HbT, CBV and SO_2 (i.e., R_{HbT}, R_{CBV}, $-R_{\mathrm{SO}_2}$) in the SSS, MI and MII arterioles in one stimulation block, shown as a function of time under different stimulation intensities (1, 2, 6 and 10 mA) and with a duration of 5 s. The error bars represent the standard deviations of the data from six rats. The yellow zone indicates the 5-s Stimulation-ON period. Note that the ipsilateral SSS is the SSS during the ipsilateral-side measurement, and the contralateral SSS is the same SSS during the contralateral-side measurement.

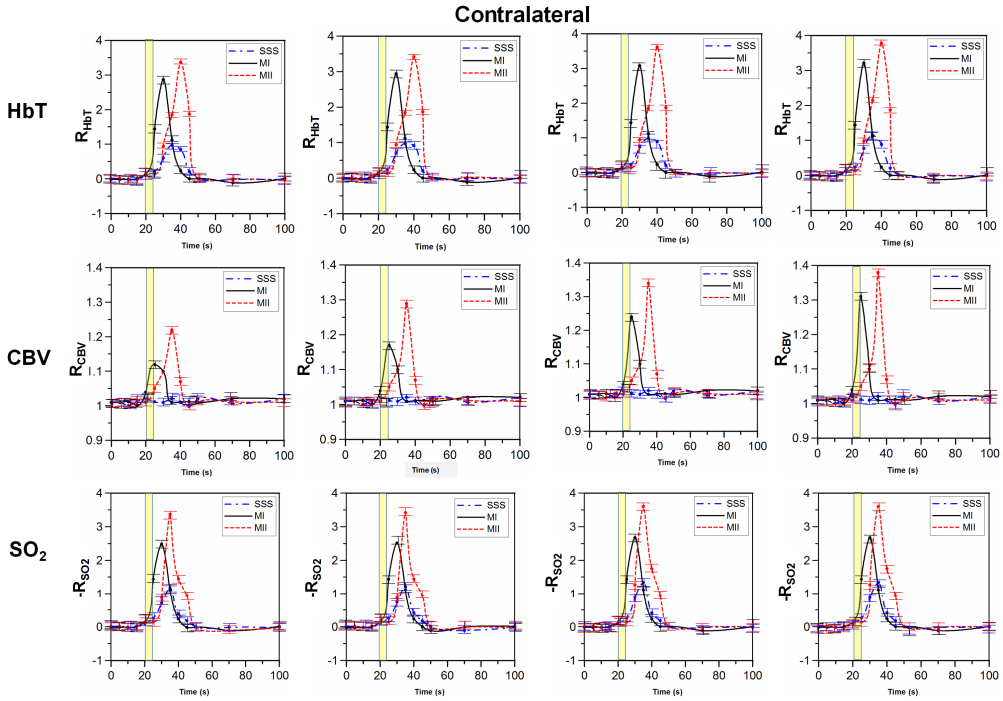

Fig. 3 Contralateral functional changes in the HbT, CBV and SO_2 (i.e., R_{HbT}, R_{CBV}, $-R_{\mathrm{SO_2}}$) in the SSS, MI and MII arterioles in one stimulation block, shown as a function of time under different stimulation intensities (1, 2, 6 and 10 mA) and with a duration of 5 s. The error bars represent the standard deviations of the data from six rats. The yellow zone indicates the 5-s Stimulation-ON period.

3.2 Functional hemodynamic changes in the bilateral cerebral vessels in response to various stimulation durations

The first column of Figure 4 show $R_{\mathrm{HbT}}(t)$ in the SSS and bilateral MI and MII arterioles in one 15-s stimulation block using a stimulation intensity of 2 mA. In this long stimulation, the time to peak R_{HbT} after stimulation onset in the SSS and the contralateral MI and MII arterioles was 18.41, 17.12 and 21.08 s, respectively. The times to peak R_{HbT} in the SSS and the contralateral MI and MII arterioles were longer than those using the 5-s stimulation. During stimulation, the peak R_{HbT} value using a 15-s stimulation was 1.16 ± 0.001 (mean ± SD) ($p < 0.001$) in the SSS, 3.240 ± 0.003 (mean ± SD) ($p < 0.001$) in the contralateral MI arteriole and 3.890 ± 0.004 (mean ± SD) ($p < 0.001$) in the MII arteriole (Wilcoxon matched-pairs signed-rank test, $n = 6$). The peak R_{HbT} values were significantly higher when the 15-s stimulation was used than when the values from the 5-s stimulation were used.

The second column of Figure 4 shows the $R_{CBV}(t)$ in the SSS and bilateral MI and MII arterioles in one stimulation block under 15-s stimulation. Using the long stimulation condition, the R_{CBV} response times from the stimulation onset to the return of R_{CBV} to baseline were 17.85 and 22.38 s for the contralateral MI and MII arterioles, respectively. The third column of Figure 4 shows $-R_{\mathrm{SO_2}}$ in the SSS and bilateral MI and MII arterioles in 1 15-s block using a 2-mA stimulation. For long stimulations, the time to peak $-R_{\mathrm{SO_2}}$ in the SSS and the contralateral MI and MII arterioles was 15.51, 15.14 and 18.89 s, respectively, after stimulation onset. The peak $-R_{\mathrm{SO_2}}$ values using the 15-s stimulation were 1.12 ± 0.001 (mean ± SD) ($p < 0.001$) in the SSS, 3.140 ± 0.002 (mean ± SD) ($p < 0.001$) in the contralateral MI arteriole and 3.840 ± 0.005 (mean ± SD) ($p < 0.001$) in the MII arteriole (Wilcoxon matched-pairs signed-rank test, $n = 6$). Using the long stimulation condition, the $-R_{\mathrm{SO_2}}$ response times from stimulation onset to the return of $-R_{\mathrm{SO_2}}$ to baseline were

27.62, 24.95 and 26.27 s in the SSS and the contralateral MI and MII arterioles, respectively. The time to peak $-R_{SO_2}$ in the contralateral MI arteriole was longer under the 15-s stimulation than the 5-s stimulation. However, the times to peak $-R_{SO_2}$ in the SSS and contralateral MII arterioles did not differ between the 15- and 5-s stimulations.

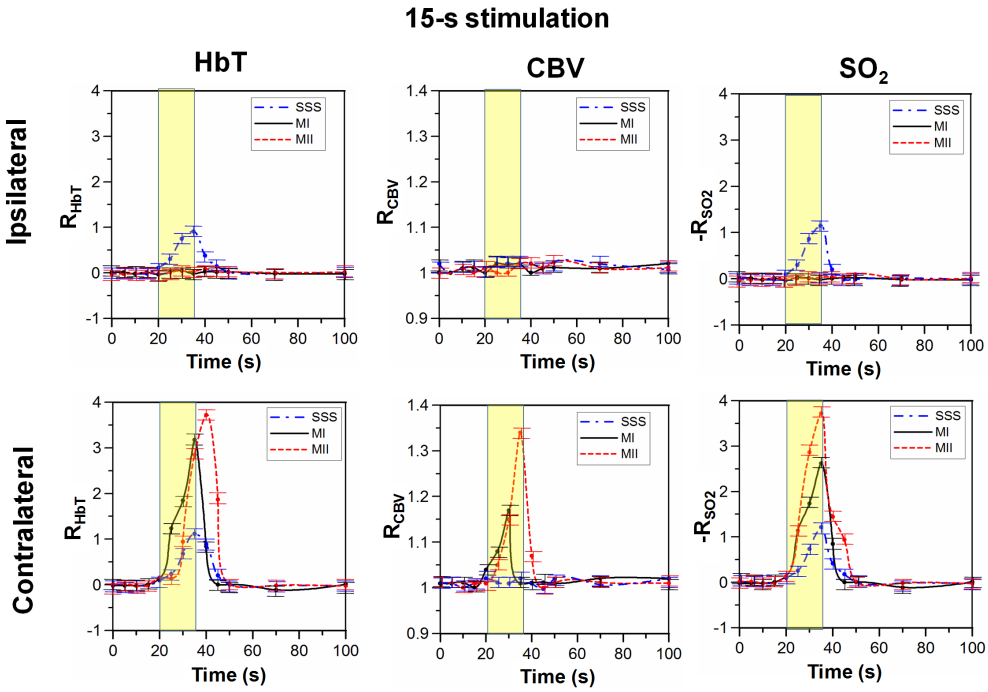

Fig. 4 Functional HbT, CBV and SO_2 changes (i.e., R_{HbT}, R_{CBV}, $-R_{SO_2}$) in the SSS and bilateral MI and MII arterioles in one stimulation block as a function of time using 15-s stimulations of 2 mA. The error bars represent the standard deviations of the data from six rats. The yellow zone indicates the Stimulation-ON period.

4. CONCLUSIONS

In summary, the present study demonstrates the unique capabilities of a fPAM system for characterizing the HRF changes in single cerebral blood vessels. Local relative functional HRFs (i.e., HbT, CBV, and SO_2) in single blood vessels using different stimulation intensities (1, 2, 6 and 10 mA) and durations (5 s and 15 s) were comprehensively analyzed and discussed. Our findings are concordant with those reported in the literature, indicating that the regulation of hemodynamic changes in single blood vessels can be reliably studied by fPAM without the use of contrast agents. The current fPAM system will be useful as a complementary modality to other neurovascular imaging techniques for label-free investigations of HRFs to assess neuronal activity in single cerebral blood vessels.

ACKNOWLEDGEMENTS

We acknowledge the National Science Council, R.O.C., for its support of this research (NSC Nos. 97-2221-E-007-084-MY3, NSC 100-2221-E-007-010-MY2, 96-2220-E-009-029, 97-2220-E-009-029, 99-2221-E-009-154 and 99-2911-I-009-101), as well as funding support from the National Tsing Hua University (Boost program 98N2531E1) and the Ministry of Education, Taiwan.

REFERENCES

[1] H. Dehghani, S. Srinivasan, B. W. Pogue and A. Gibson, "Numerical modelling and image reconstruction in diffuse optical tomography," *Philosophical Transactions of the Royal Society A: Mathematical, Physical and Engineering Sciences,* vol. 367, pp. 3073-3093, 2009.

[2] L. V. Wang and H.-i. Wu, *Biomedical Optics: Principles and Imaging*: Wiley, 2007.

[3] G. Gratton and M. Fabiani, "Dynamic brain imaging: event-related optical signals (EROS) measures of the time course and localization of cognitive-related activity," *Psychonomic Bulletin and Review,* vol. 5, pp. 535-563, 1998.

[4] M. B. Bouchard, B. R. Chen, S. A. Burgess and E. M. C. Hillman, "Ultra-fast multispectral optical imaging of cortical oxygenation, blood flow, and intracellular calcium dynamics," *Optics Express,* vol. 17, pp. 15670-15678, 2009.

[5] P. Miao, N. Li, N. V. Thakor and S. Tong, "Random process estimator for laser speckle imaging of cerebral blood flow," *Optics Express,* vol. 18, pp. 218-236, 2010.

[6] N. Li, X. Jia, K. Murari, R. Parlapalli, A. Rege and N. V. Thakor, "High spatiotemporal resolution imaging of the neurovascular response to electrical stimulation of rat peripheral trigeminal nerve as revealed by in vivo temporal laser speckle contrast," *Journal of Neuroscience Methods,* vol. 176, pp. 230-236, 2009.

[7] M. Peng, A. Rege, L. Nan, N. V. Thakor and T. Shanbao, "High resolution cerebral blood flow imaging by registered laser speckle contrast analysis," *IEEE Transactions on Biomedical Engineering,* vol. 57, pp. 1152-1157, 2010.

[8] H. F. Zhang, K. Maslov and L. V. Wang, "In vivo imaging of subcutaneous structures using functional photoacoustic microscopy," *Nature Protocols,* vol. 2, pp. 797-804, 2007.

[9] S. A. Ermilov, T. Khamapirad, A. Conjusteau, M. H. Leonard, R. Lacewell, K. Mehta, T. Miller and A. A. Oraevsky, "Laser optoacoustic imaging system for detection of breast cancer," *Journal of Biomedical Optics,* vol. 14, p. 024007, 2009.

[10] H. F. Zhang, K. Maslov, G. Stoica and L. V. Wang, "Functional photoacoustic microscopy for high-resolution and noninvasive in vivo imaging," *Nature Biotechnology,* vol. 24, pp. 848-851, 2006.

[11] L. V. Wang, "Multiscale photoacoustic microscopy and computed tomography," *Nature Photonics,* vol. 3, pp. 503-509, 2009.

[12] L.-D. Liao, M.-L. Li, H.-Y. Lai, Y.-Y. I. Shih, Y.-C. Lo, S. Tsang, P. C.-P. Chao, C.-T. Lin, F.-S. Jaw and Y.-Y. Chen, "Imaging brain hemodynamic changes during rat forepaw electrical stimulation using functional photoacoustic microscopy," *NeuroImage,* vol. 52, pp. 562-570, 2010.

[13] G. Paxinos, Watson, Charles, *The rat brain in stereotaxic coordinates*. San Diego: Academic Press, 2007.

[14] Y.-Y. Chen, Y.-Y. I. Shih, Y.-C. Lo, P.-L. Lu, S. Tsang, F.-S. Jaw and R.-S. Liu, "MicroPET imaging of noxious thermal stimuli in the conscious rat brain," *Somatosensory & Motor Research,* vol. 27, pp. 69-81, 2010.

[15] B. P. Chugh, J. P. Lerch, L. X. Yu, M. Pienkowski, R. V. Harrison, R. M. Henkelman and J. G. Sled, "Measurement of cerebral blood volume in mouse brain regions using micro-computed tomography," *NeuroImage,* vol. 47, pp. 1312-1318, 2009.

[16] G. Paxinos, *The rat nervous system*, Third Edition ed., 2004.

[17] R. Weber, P. Ramos-Cabrer, C. Justicia, D. Wiedermann, C. Strecker, C. Sprenger and M. Hoehn, "Early Prediction of Functional Recovery after Experimental Stroke: Functional Magnetic Resonance Imaging, Electrophysiology, and Behavioral Testing in Rats," *Journal of Neuroscience,* vol. 28, pp. 1022-1029, 2008.

[18] J. B. Mandeville, J. J. Marota, C. Ayata, M. A. Moskowitz, R. M. Weisskoff and B. R. Rosen, "MRI measurement of the temporal evolution of relative CMRO2 during rat forepaw stimulation," *Magnetic Resonance in Medicine,* vol. 42, pp. 944-951, 1999.

[19] A. C. Silva, S.-P. Lee, G. Yang, C. Iadecola and S.-G. Kim, "Simultaneous blood oxygenation level-dependent and cerebral blood flow functional magnetic resonance imaging during forepaw stimulation in the rat," *Journal of Cerebral Blood Flow & Metabolism,* vol. 19, pp. 871-879, 1999.